Bulletin of Mathematical Biology (1999) **61**, 113–140
Article No. bulm.1998.0080
Available online at http://www.idealibrary.com on IDEAL

A Mathematical Model for Simulating Virus Transport through Synthetic Barriers

MATTHEW R. MYERS, C. DAVID LYTLE, LICIA B. ROUTSON
Center for Devices and Radiological Health,
U.S. FDA, HFZ-132,
12725 Twinbrook Parkway,
Rockville,
MD 20852, U.S.A
E-mail: mrm@cdrh.fda.gov

Synthetic barriers such as gloves, condoms and masks are widely used in efforts to prevent disease transmission. Due to manufacturing defects, tears arising during use, or material porosity, there is inevitably a risk associated with use of these barriers. An understanding of virus transport through the relevant passageways would be valuable in quantifying the risk. However, experimental investigations involving such passageways are difficult to perform, owing to the small dimensions involved. This paper presents a mathematical model for analyzing and predicting virus transport through barriers. The model incorporates a mathematical description of the mechanisms of virus transport, which include carrier-fluid flow, Brownian motion, and attraction or repulsion via virus–barrier interaction forces. The critical element of the model is the empirically determined rate constant characterizing the interaction force between the virus and the barrier. Once the model has been calibrated through specification of the rate constant, it can predict virus concentration under a wide variety of conditions. The experiments used to calibrate the model are described, and the rate constants are given for four bacterial viruses interacting with a latex membrane in saline. Rate constants were also determined for different carrier-fluid salinities, and the salt concentration was found to have a pronounced effect. Validation experiments employing laser-drilled pores in condoms were also performed to test the calibrated model. Model predictions of amount of transmitted virus through the drilled holes agreed well with measured values. Calculations using determined rate constants show that the model can help identify situations where barrier-integrity tests could significantly underestimate the risk associated with barrier use.

1. INTRODUCTION

In recent years, concern about the AIDS epidemic has led to a substantial increase in attention towards barriers to virus transmission. The most commonly used barriers are gloves (surgical and examination) and condoms, but endoscopic sheaths, biomedical filters, gowns, drapes, and masks also constitute barriers of considerable public-health importance. Due to material or manufacturing defects, holes and

0092-8240/99/020113 + 28 $30.00/0

tears which arise during barrier use, and material porosity, a nonzero likelihood of transmission through the barrier inevitably exists. Tests are therefore necessary to evaluate barrier effectiveness. These tests often incorporate a membrane filled with a virus suspension under static pressure (Lytle *et al*., 1991; Carey *et al*., 1992), and the viruses transmitted into a collection fluid outside the membrane are counted. While providing valuable data on the barrier integrity under a specific set of test conditions, the penetration tests also motivate a number of critical questions regarding barrier effectiveness under more general circumstances. For example, given the probability of transmission of a certain virus through a membrane, what is the probability of transmission of a different (potentially more hazardous) virus? Or what is the likelihood of transmission under nonstatic conditions? In essence, when do penetration tests underestimate the risk associated with the use of a given barrier?

An understanding of the mechanisms of virus transport through barrier pores would be valuable in accurately predicting barrier performance. (We will use the term pore to signify passageways of all types.) Unfortunately, experimental investigation of virus motion within pores is very difficult, owing to the small dimensions involved. In this paper we present an alternative method for studying virus transport through barriers, in the form of a computational model. The model incorporates a mathematical description of the three dominant mechanisms of virus transport—flow of the carrier fluid (saline, blood, semen, etc.), random thermal motion, and short-range virus–barrier interaction forces—into conservation equations to yield the virus concentration throughout a prescribed pore geometry.

While mathematical models of particle transport through pores have been applied to many industrial filtering processes, to our knowledge such models have not been applied to virus permeation through synthetic barriers. This void is largely due to the lack of knowledge about the interaction forces between the virus and pore surface, and about how the characteristics of the carrier fluid affect the interaction forces. Much of the effort of the present study has been devoted to characterizing experimentally the virus–barrier interaction forces.

Besides the information characterizing the interaction forces, other inputs to the model include virus size, virus concentration at the inlet of the pore, and pressure driving the virus suspension through the pore. In laboratory tests of barriers, the driving pressure is typically known, though in practice (i.e., during actual barrier use) it must sometimes be roughly estimated from physiological information or treated as a variable in a parametric study. The final input required by the model is a geometric representation of the pore. The pore geometry is often unknown in practice; hence, a complete prediction model should be capable of examining a variety of possible pore types—tubes of various cross-sectional shapes, tortuous paths, porous media, etc. Once the input information has been specified, the particle-transport equations are numerically solved in the prescribed geometry to yield the virus concentration throughout the pore, most importantly at the outlet.

In this introductory study, the viruses considered were the bacterial viruses (bacteriophages) ϕX174, PRD1, ϕ6, and MS2. The bacteriophages are laboratory-safe,

comparable in size to many viruses of public-health importance, including HIV and the Hepatitis viruses, and are used as surrogates for human viruses in laboratory tests of barriers (Lytle and Routson, 1995). Additionally, $\phi 6$ contains an external lipid membrane, like HIV. The barrier material used in our experiments was latex, due to its pervasiveness in disease prevention. Saline was the carrier fluid throughout, though the salt concentrations were varied to observe the effect of carrier-fluid composition on the electrical forces. Pore geometries were limited to the parallel-plate configuration of the calibration apparatus and the circular-cylinder geometry characterizing the laser-drilled pores in condoms used to test the calibrated model.

The next section develops the mathematical foundations for the computational model. Section 3 then describes the calibration experiments used to provide the critical input to the model, the rate constant characterizing the virus–barrier interaction forces. Once the rate constant is specified for a particular virus–barrier–carrier-fluid combination, the model is calibrated for that combination and is capable of predicting the amount of virus transmitted under a wide variety of conditions. In Section 4 we discuss the validation experiments used to test the model under conditions different from those used during calibration. Section 5 provides results of the calibration and validation experiments as well as predictions for amounts of transmitted virus in situations of potential public-health importance. The important features of the results, including implications of model predictions on the risk associated with barrier use, are discussed in Section 6. Section 7 summarizes the major results and outlines future directions for model development.

2. MATHEMATICAL FORMULATION

The mechanisms by which viruses are transported through a barrier pore are threefold. The first is convection due to the flow of fluid in which the viruses are suspended. In essentially all barrier tests there is a net flow of the carrier fluid due to an imposed pressure gradient. (Initiation of the flow is likely influenced by surface tension as well.) In general, the viruses will both translate and rotate due to their hydrodynamic interaction with the carrier fluid. The second mechanism of virus transport is random thermal motion, or Brownian motion. Brownian motion is typically negligible in the direction of fluid flow but is the dominant transport mechanism direction perpendicular to the fluid streamlines. If the residence time of the viruses within the pore is sufficiently long, Brownian motion enables them to migrate to the boundary and experience a short-range interaction force exerted by the pore surface. Whether the viruses subsequently adsorb to the pore surface depends upon the extent of attraction or repulsion of the force as a function of distance. The mechanisms of virus transport are summarized schematically in Fig. 1.

The transported quantity of interest is the virus concentration (number of viruses per unit volume), denoted as $c(x_i, t)$, where x_i is tensor notation for the coordinate vector (x_1, x_2, x_3) and t is time. In the absence of any sources of viruses within the

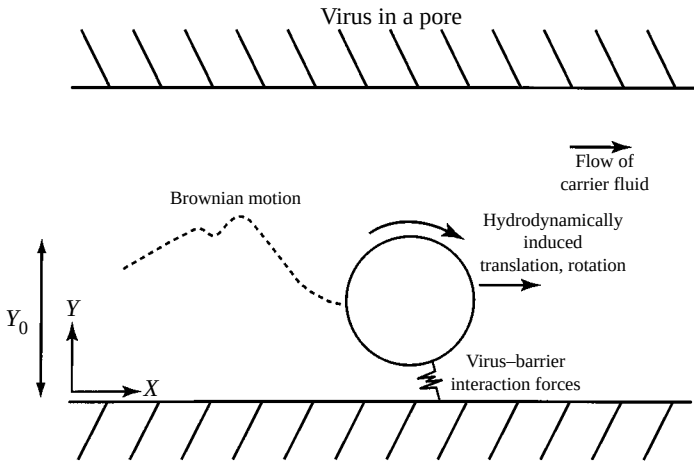

Figure 1. Mechanisms of virus transport within a pore.

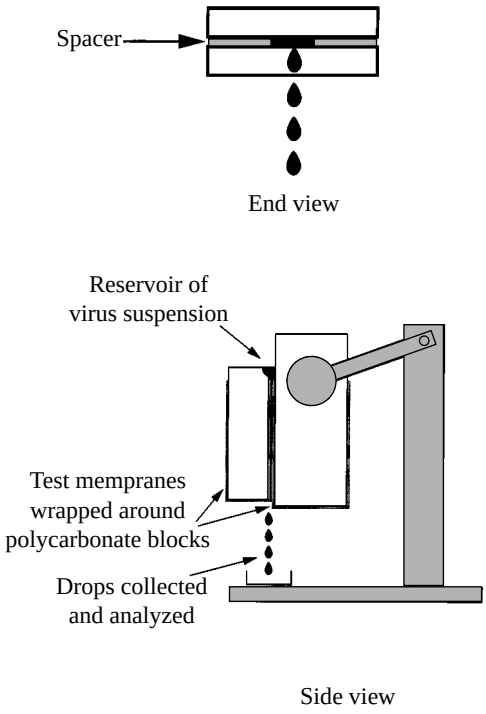

Figure 2. Parallel-sheet apparatus used in calibration experiments.

pore, the virus concentration obeys the standard conservation equation

$$\frac{\partial c}{\partial t} + \frac{\partial}{\partial x_i} J_i = 0, \tag{1a}$$

where J_i is the virus flux and summation over repeated indices is implied. The flux is the sum of the convective term, the Brownian or diffusion term, and the contribution from interaction forces (Brenner and Gaydos, 1977):

$$J_i = cV_i - D_{ij}\frac{\partial c}{\partial x_j} + c\frac{D_{ij}}{kT}F_j. \tag{1b}$$

Here V_i is the virus velocity, D_{ij} the diffusivity tensor characterizing the Brownian motion, k the Boltzmann constant, T the absolute temperature, and F_j any external force. The virus velocity V_i is related to but different from the fluid velocity which would exist in the pore at the same location in the absence of the virus. Under most general circumstances, the virus and fluid velocities are obtained by solving the equations of motion for a translating and rotating particle simultaneously with the equations for a fluid flowing inside a pore and around the particle. The solutions are coupled by the requirement that the fluid and particle velocities match at the fluid–particle interface. This procedure must be followed when the virus size is comparable to the cross-sectional dimension of the pore.

The boundary condition imposed at the pore surface is the perfect-sink condition:

$$c = 0 \qquad \text{on pore surface.} \tag{2a}$$

This statement implies that viruses in contact with the pore surface are immobilized, i.e., the concentration of free viruses at the pore surface is zero. The condition also implies that the pore surface can accommodate infinitely many viruses which may adsorb to it, without changing concentration, analogous to a perfect thermal sink. The perfect-sink boundary condition has been used extensively in colloidal-particle transport theory (Bowen *et al.*, 1976; Prieve and Lin, 1980; Adamczyk and Van De Ven, 1981; Chari and Rajagopalan, 1985; Song and Elimelech, 1995), but as pointed out by Van de Ven (1989), the perfect-sink condition is limited in its ability to model realistically particle–wall interactions. The perfect-sink condition cannot account for reversibility (desorption of the particles back into the suspension) or dynamic adsorption (motion of particles constrained in the direction normal to the wall by interaction forces but able to move slowly in the direction parallel to the wall). However, because of its inherent simplicity and, as we will see, usefulness in predicting experimental results under a range of conditions of practical importance, we retain the perfect-sink condition. The limitations of the model resulting from application of the perfect-sink boundary condition are discussed in Section 6.

At the pore inlet, the virus concentration is prescribed:

$$c = c_0 \qquad \text{at inlet.} \tag{2b}$$

At the outlet of the pore the normal derivative of the concentration, i.e., the diffusive flux, is assumed to be zero:

$$\nabla c \cdot \boldsymbol{n} = 0 \qquad \text{at outlet.} \tag{2c}$$

Even without consideration of complicated virus–barrier interaction forces, equations (1) and (2) are essentially untractable for arbitrary virus and pore sizes and shapes. To proceed further we make several simplifying assumptions, and to help justify these and subsequent assumptions we consider three scenarios to which the model will be applied. The first scenario is a calibration experiment (described in the next section): between two parallel sheets of latex a virus suspension flows under gravity. The second is a validation experiment (described in Section 4), in which the virus suspension flows through a drilled hole in a latex membrane. The third scenario is virus transport through a hypothetical 1-μm diameter hole in a latex membrane, under the influence of an 80 000 dynes cm^{-2} driving pressure. The 80 000 dynes cm^{-2} value is based upon coital simulations and is used in standard FDA barrier tests (Carey *et al*., 1992) The 1-μm diameter considered is the order-of-magnitude hole size observed in the fraction of surgical gloves found to leak in a recent study (Lytle *et al*., 1991), assuming the holes yielding the observed amount of transmitted virus are circular. Values of the relevant parameters for the three scenarios are provided in Table 1. The simplifying assumptions and observations we incorporate into the model are the following:

(1) The virus is spherical. This is approximately true for many viruses of public-health importance, including HIV.

(2) The virus diameter is small (but not necessarily negligible) relative to the pore diameter. (We use the term diameter to denote the cross-sectional characteristic dimension of the pore, even though the cross-section is rarely circular.) This assumption, when combined with assumption (1), allows for treatment of the virus near the pore wall as a sphere near a plane. While the virus diameter is assumed small compared to the pore dimension, it is taken to be large relative to the molecular size of the carrier fluid (e.g., water), so that the virus may be treated as a particle suspended in a fluid continuum.

(3) The carrier fluid is assumed to be Newtonian. This is a reasonable assumption for saline, but the model may require modification in order to treat blood or semen as the carrier fluid.

(4) Gravitational and hydrodynamic lift forces on the viruses can be neglected. Because of the minute size of the viruses, forces proportional to their mass, and hence the cube of their diameter, can be neglected. Typical gravity numbers are provided in Table 1.

(5) The interaction force between the virus and pore acts normal to the pore surface, and is a function strictly of the separation between the virus and the mean surface of the pore wall. The pore surface must therefore be sufficiently smooth on the scale of the virus diameter.

(6) Interactions between viruses can be neglected. This requires a sufficiently dilute virus suspension.

(7) Steady-state conditions are assumed to apply. As discussed in Section 6, the transmission rate through the calibration apparatus was observed to be steady, even for high adsorption rates. (The number immobilized viruses adsorbed to the pore

Table 1. Parameter values for three barrier-use scenarios: (1) The calibration experiments, wherein the virus suspension descends under the influence of gravity, between two parallel sheets of barrier materials; (2) The validation experiments, in which the virus suspension flows through a laser-drilled hole in a barrier, with a driving pressure of 5400 dynes cm^{-2}; and (3) Transport through a 1 μm hole in a latex barrier, under the influence of a driving pressure of 80 000 dynes cm^{-2}.

Parameter values in three barrier-use scenarios				
Parameter	Unit	Scenario 1	Scenario 2	Scenario 3
Virus radius a	(cm)	0.000005	0.000005	0.000005
Pore dimension y_0 or r_0	(cm)	0.0025	0.0001	0.00005
Pore length L	(cm)	15	0.01	0.01
Pressure gradient $\frac{\partial p}{\partial x}$	(dynes cm^{-3})	980	540 000	8 000 000
Carrier-fluid viscosity μ	(poise)	0.01	0.01	0.01
Carrier-fluid density ρ	(gm cm^{-3})	1.0	1.0	1.0
Mean axial fluid velocity V_m	(cm s^{-1})	0.2	0.08	0.25
Virus Diffusivity D_∞	(10^{-8} cm^2 s^{-1})	4.3	4.3	4.3
Peclet Number $\frac{V_m y_0}{D_\infty}$		11 000	200	300
Reynolds Number $\frac{V_m y_0 \rho}{\mu}$		0.05	0.0009	0.0012
Gravity Number $\frac{4\pi\rho g a^4}{3kT}$		0.0005	0.0005	0.0005

wall increases with time, but not number of viruses able to contribute to the flux through the pore.)

As an example of the application of equations (1) and (2) and the simplifying assumptions, we now develop the reduced equations in the Cartesian coordinate system appropriate for the calibration apparatus described in the next section. The virus suspension flows between two parallel sheets which are effectively infinite in the transverse dimension (the ratio of the transverse dimension of the sheets to the separation between them is about 200:1), i.e., the problem is approximately two-dimensional. The geometry and (x, y) axes are pictured in Fig. 1. For the small Reynolds numbers (Table 1) typically arising in flows through membrane pores, there is a short developing region at the pore inlet, after which the fluid and virus velocities are entirely in the x-direction and dependent only upon y. We therefore neglect the virus transverse velocity component V_2 and abbreviate the axial velocity $V_1(y)$ as $V(y)$. Likewise, the virus diffusivity components become dependent solely upon y just beyond the pore inlet. [For a sphere in the vicinity of a plane wall, only the diagonal elements D_{11} and D_{22} (and D_{33} for three-dimensional analyses) of the diffusivity tensor are nonzero (Brenner and Leal, 1977).] Finally, the axial diffusion term $D_{11}\partial^2 c/\partial x^2$, which is of order (1/Pe)(y_0/L) (see Table 1) relative to axial convection, is ignored. (Very near the pore wall the virus velocity goes to zero and axial diffusion is comparable to axial convection, but we shall see that there transverse diffusion dominates.) In the complete absence of bulk flow through the membrane, axial diffusion must be restored.

Under these conditions, equation (1) becomes

$$V(y)\frac{\partial c}{\partial x} - \frac{\partial}{\partial y}\left(D(y)\frac{\partial c}{\partial y}\right) + \frac{\partial}{\partial y}\left(cD(y)\frac{F(y)}{kT}\right) = 0. \tag{3}$$

Here D and F are abbreviations for the diffusivity tensor component D_{22} and force vector normal component F_2, respectively. The inlet of the parallel-sheet pore is located at $x = 0$, the outlet at $x = L$. The lower sheet is in the plane $y = 0$ and the pore half-height (i.e., the line of symmetry) is defined by $y = y_0$. The virus is located by the position of its center, so the range of allowable vertical positions for the virus is $y \in (a, 2y_0 - a)$, where a is the virus radius. The boundary conditions simplify to

$$c(x, a) = 0, \tag{4a}$$

$$\frac{\partial c}{\partial y}(x, y_0) = 0, \tag{4b}$$

$$c(0, y) = c_0. \tag{4c}$$

Condition (4b) is a statement of symmetry across the pore centerline $y = y_0$.

The virus velocity $V(y)$ in (3) takes the form

$$V(y) = V_f(y) g_1(y), \tag{5a}$$

where $V_f(y)$ is the fluid velocity, which for fully developed flow through the parallel-sheet configuration is given by

$$V_f(y) = \frac{3}{2} V_m \left(\left(\frac{y}{y_0} \right)^2 - 2 \frac{y}{y_0} \right). \tag{5b}$$

Here

$$V_m = \frac{y_0^2}{3\mu} \left(-\frac{\partial p}{\partial x} \right) \tag{5c}$$

is the mean velocity across the channel, μ the carrier-fluid viscosity, and $\partial p/\partial x$ the pressure gradient along the pore axis. (The pressure decreases with increasing axial distance, making $\partial p/\partial x$ negative.) The resistance factor $g_1(y)$ accounts for hydrodynamic interaction of the wall with the virus and is given in tabulated form by Goldman *et al.* (1967). Beyond a few virus diameters from the pore wall $g_1(y)$ is equal to one, while as the gap between the virus and wall shrinks to 0, $g_1(y)$ behaves as:

$$g_1(y) \sim \frac{0.7431}{0.6376 - 0.2\ln(h)} \qquad (h \to 0), \tag{5d}$$

where

$$h = \frac{y - a}{a} \tag{5e}$$

is the dimensionless gap between the virus perimeter and the pore surface. Hence the virus velocity decays to zero inversely as the logarithm of the pore–virus separation. The pore boundaries likewise affect the virus diffusivity; it has the form

$$D(y) = D_\infty g_2(y), \tag{6a}$$

where D_∞ is the diffusivity for a Brownian particle of radius a in an unbounded medium (Probstein, 1994):

$$D_\infty = \frac{kT}{6\pi\mu a}. \tag{6b}$$

The function $g_2(y)$ decays linearly to zero as the gap shrinks:

$$g_2(y) \sim h \qquad (h \to 0), \tag{6c}$$

demonstrating that the random thermal motion is hindered by the presence of the walls. Away from the wall ($h \gg 0$)g_2 attains the value of 1, and for intermediate h values g_2 has been tabulated by Brenner and Gaydos (1977).

The function $F(y)$ represents the force between the virus and the barrier in the presence of the carrier fluid. In the most general case this force is quite complicated, particularly as the virus–barrier separation approaches molecular dimensions, where the continuum approximation breaks down. Short range (on the order of a nanometer) solvation forces (Israelachvili, 1992), which are not describable by a continuum model, determine the nature of the adhesion between the pore and the virus. For the purpose of virus-transport modeling, determination of the ultimate fate of the virus is not paramount, and we consider viruses approaching to within molecular dimensions of the boundary to be adsorbed into a perfect sink. We turn our attention to the longer-ranging forces which govern whether the virus is attracted to the pore surface. To a good approximation these forces are the van der Waals and electrical double layer forces, which form the basis of the DLVO theory (Hiemenz, 1986) used very successfully in modeling colloid stability and particle capture. The virus–barrier interaction forces are significant roughly on the scale of the particle diameter, and hence are long-range on the molecular scale but short-range on the scale of the pore diameter.

The van der Waals force arises due to the electrical dipole distributions within two interacting bodies. The magnitude and sign of the force depends upon the nature of the propagation medium between the objects, but the van der Waals force is usually attractive. This is the case for all of the viruses we have considered interacting with latex in a saline medium. An expression for the van der Waals force valid at all separation distances cannot in general be written, particularly if the finite propagation time of the electromagnetic field between the interacting

bodies is accounted for. A simple expression for the force between a sphere and a plane wall, valid for gap distances less than about 15 nm, is

$$F_{vdw} = -\frac{2A}{3a}\frac{1}{h^2(h+2)^2}. \tag{7}$$

The parameter A, known as the Hamaker constant, takes on values about $10^{-20}\,J$ in magnitude. Other expressions for the van der Waals force, having different ranges of validity, are given by Jia and Williams (1990).

The electrical double layer force is present when there is a net electrical charge on two interacting bodies. Membranes and viruses in an aqueous medium near neutral pH are normally negatively charged; hence a repulsive electrical (Coulombic) force exists. Mathematical description of the electrical force is difficult, as the source term in the Poisson equation governing the electric potential is nonlinearly related to the electric potential, through the Boltzmann distribution describing the ion concentration within the carrier fluid. Uncertainty over whether a constant-charge or constant-potential approximation applies as the virus approaches the pore wall also contributes to the inexactitude of the mathematical description. The following result of Hogg *et al.* (1966) has been shown to be reasonably accurate for surface potentials up to 60 mV:

$$F_{edl} = \pi\epsilon_0\epsilon_r a\kappa\left(2\psi_1\psi_2\frac{2\exp(-\kappa h)}{1-\exp(-2\kappa h)} - (\psi_1^2+\psi_2^2)\frac{2\exp(-2\kappa h)}{1-\exp(-2\kappa h)}\right), \tag{8}$$

where ϵ_0 is the dielectric permittivity in vacuum, ϵ the relative permittivity of the carrier fluid, κ the reciprocal Debye length, and ψ_1 and ψ_2 the surface electric potentials of the virus and membrane. The range of validity of (8) and other approximations to the electrical force is discussed by Rajagopalan and Kim (1981) and Jia and Williams (1990).

The total interaction force $F = F_{vdw} + F_{edl}$ contains three empirical parameters, the Hamaker constant A characterizing the van der Waals force and the two electric potentials ψ_1 and ψ_2. [The Debye length κ is also unknown but can be computed from the ion concentration within the carrier fluid (Hiemenz, 1986).] Unfortunately, for viruses, barriers, and carrier fluids of interest none of these parameters is typically known. Hence it was initially an objective of this study to determine empirically all three parameters for each virus–barrier–carrier-fluid combination. The calibration experiments described in the next section were begun with this three-dimensional parameter-estimation as the goal. Calibration of the model was to be performed by finding the three parameters which minimized the difference between the measured and computed amounts of virus transmission. However it was discovered that the singular behavior of the interaction force necessitated an extremely dense computational grid (the numerical methods are discussed below) near the boundary. The computational time required to span the three-dimensional

parameter space was consequently quite long. The following boundary-layer approach, adopted to treat analytically the rapid behavior near the pore wall and thereby reduce computational time, also had profound implications on the amount of empirical information required to calibrate the model.

In order to examine the dynamics of virus transport in a small region near the pore wall scaling on the virus size, we can order the various terms in (3) by nondimensionalizing the transverse lengths by the virus radius a. The velocity in this boundary layer is of order $V_m(a/y_0)$ in magnitude [equation (5b)]. Relative to transverse diffusion, which is given by the second term in (3), axial convection [first term in (3)] is of order $(\mathrm{Pe})(a/y_0)^3(y_0/L)$. Based on the values in Table 1, this product is very small. Thus, despite the high Peclet numbers typically characterizing virus transport, over the small dimensions in which the interaction force is important, convective transport can be ignored. Axial diffusion, if included in (3), is roughly $(a/L)^2$ times smaller than transverse diffusion, and is likewise insignificant. The interaction-force term, the third term in (3), is $O(1)$ relative to transverse diffusion. We therefore retain the first and third terms in (3), and after integrating the reduced equation with respect to y we obtain

$$D(y)\frac{\partial c_{bl}}{\partial y} - c_{bl}D(y)\frac{F(y)}{kT} = -J_2(x). \tag{9}$$

The subscript bl denotes boundary-layer quantities. The function of integration $J_2(x)$ is the virus flux toward the boundary, since the convective term in (1b) is neglected in the boundary layer. Integrating (9) once more with respect to y and enforcing boundary condition (4a) yields:

$$c_{bl} = -J_2(x)\exp(-\phi(y)/kT)\int_a^y \frac{\exp(\phi(y')/kT)}{D(y')}\,dy'. \tag{10}$$

The function ϕ is the potential energy associated with the force F, i.e., $F(y) = -\partial\phi/\partial y$.

In the outer region beyond the boundary layer, the interaction forces are zero and (3) reduces to

$$V(y)\frac{\partial c_{out}}{\partial x} - \frac{\partial}{\partial y}\left(D(y)\frac{\partial c_{out}}{\partial y}\right) = 0. \tag{11}$$

The approach of $D(y)$ to its asymptotic value (D_∞) as y increases is slower than that of $F(y)$; hence the dependence of D on y is retained in the outer region. As virus motion due to virus–barrier interaction forces is absent in the outer region, and the virus velocity component normal to the wall due to bulk fluid flow is zero, the normal flux is simply

$$J_{2,out} = -D(y)\frac{\partial c_{out}}{\partial y}. \tag{12}$$

In the case of a nonzero normal velocity at the edge of the boundary layer, as in a stagnation-point flow, the normal convective flux cV_2 must be small compared with the diffusive flux $D\partial c/\partial y$ in order to apply the present theory. At the edge of the boundary layer, the normal convective flux is $O(V_2 a/D_\infty)$relative to diffusion. For a stagnation-point flow around a sphere of radius a_s (representing the characteristic scale of the medium), the velocity V_2 is $O((a/a_s)^2)$ relative to the freestream velocity V_∞ (Probstein, 1994). Hence it is required that $V_\infty a^3/D_\infty a_s^2$ be small when bulk flow normal to the boundary is present.

At the edge of the boundary layer, both the virus concentration and the normal flux must be continuous. After evaluating (10) at the boundary-layer limit, denoted by $y = y_{bl}$, and using the continuity conditions in conjunction with (12) to replace inner variables by outer ones, we have the outer boundary condition

$$Kc_{out}(x, y_{bl}) - D(y_{bl})\frac{\partial c_{out}}{\partial y}(x, y_{bl}) = 0, \tag{13}$$

where

$$K^{-1} = \exp(-\phi(y_{bl})/kT)\int_a^{y_{bl}} \frac{\exp(\phi(y')/kT)}{D(y')}dy'. \tag{14}$$

Selection of y_{bl} is discussed subsequently.

As the axial virus flux within the boundary layer is small, for the purpose of computing virus transmission through a pore the virus concentration can be determined using just the outer equations, (11), (4b), (4c), and (13). Equation (13) states that the virus transport within the boundary layer can be viewed as a first-order reaction occurring at $y = y_{bl}$, with rate constant K (Bowen *et al.*, 1976). The outer equations exhibit no rapid variations and can be solved much more quickly than the full equations. But more importantly than providing an increase in computational efficiency, the boundary layer approach has reduced the number of required empirical parameters to one, the rate constant K. The relevant K values can be determined directly from the experiments, rather than indirectly by computing the interaction-force parameters (A, ψ_1, ψ_2) and using them to perform the calculation in (14). Hence, even though expressions for the van der Waals and electrical forces over the entire range of interest may be unwieldy, and contain questionable assumptions in certain circumstances, these complications are irrelevant if we work directly in terms of rate constants.

The procedure for determining K was: given the calibration-apparatus dimension y_0 and the measured relative transmission (amount of virus out of the channel for a specified time period divided by the amount in), solve the outer equations in the simulated geometry, compute the relative transmission, and adjust K until the relative transmissions agree to a small tolerance. The relative transmission was determined computationally from the ratio of the integrated fluxes at the inlet and

outlet sections:

$$\text{relative transmission} = \frac{\int_{y_{bl}}^{y_0} c(L, y)V(y)dy}{\int_{y_{bl}}^{y_0} c(0, y)V(y)dy}. \tag{15}$$

The relative transmission allows for comparisons to be made independent of the inlet concentration, which is difficult to keep constant experimentally. The actual number of viruses transmitted in a given experiment is the numerator of (15) multiplied by the channel width and the relevant time interval. The relative transmission can also be interpreted as the probability of transmission through the pore for any given virus.

The inverse problem of determining K given relative transmission was solved using a secant method, which typically converged to 10^{-6} accuracy in approximately five iterations (i.e., five solutions to the outer equations). The outer equations were solved using finite-differences and the method of lines, as implemented in the NAG software package (Numerical Algorithms Group, 1991). The uniform spatial density in the y-direction was refined until doubling the number of grid points produced less than 0.1% change in flux through the pore. The local error tolerance in the marching (i.e., x) direction was refined in a similar manner. Using 1000 points across the channel and a local accuracy of 10^{-5} for marching axially, execution times were in the order of 1 min on a VAX 4000 computer.

To apply the reaction-rate boundary condition in the computations, specification of the boundary-layer limit y_{bl} was required. Selection of y_{bl} was based on two considerations: if y_{bl} was made too small the interaction force was not negligible outside the boundary layer, while if y_{bl} was chosen too large a significant convective flux existed within the boundary layer. To isolate the optimal boundary-layer width, solutions of the outer equations using various values of y_{bl} were compared with corresponding solutions to the full equations (3) and (4). In order to perform this comparison, it was assumed that the virus–membrane interaction forces were adequately described by (7) and (8). The full equations were solved via the same finite-difference algorithm as the reduced equations, except that an additional 1000 grid points (uniformly spaced) were required to resolve accurately the behavior within the boundary-layer. It was found that a boundary layer thickness of two virus radii, i.e., $h = 2$ or $y_{bl} = 3a$ [equation (5e)] satisfied the above two criteria quite well. Results comparing the full numerical solution with the approximate solution based upon the boundary-layer approach are provided in Section 5.

3. CALIBRATION EXPERIMENTS

The calibration apparatus was designed with two main criteria in mind:

(1) transport through the apparatus must be easy to simulate computationally, i.e., the geometry should be relatively simple,

(2) the residence time of the viruses in the apparatus cannot be too small relative to the time necessary for the viruses to diffuse across the apparatus. Otherwise, there will be insufficient time for the viruses to interact with the membrane.

The device ultimately selected, shown in Fig. 2, employed two parallel sheets of latex with the virus suspension flowing between them under gravity. The gap between the sheets was controlled by the presence of two strips of paper serving as spacers. The length of the resulting rectangular channel was 15.2 cm and its width, i.e., the distance between the spacers, was 1.0 cm. The channel height (the gap between the sheets) varied with spacer thickness and the clamping force applied perpendicular to the sheets to avoid leaks, but was about 50 μm on average. The large ratio of the channel width to height allowed for the two-dimensional approximation of the channel geometry described in Section 2. The latex sheets were obtained by wrapping commercial condoms around polycarbonate blocks, which were then clamped together with the spacer in between. (Thus, to be precise, the barriers were latex condoms with any coatings added during the fabrication processes.) The blocks were machined at the top to provide a reservoir for the virus suspension. One block was slightly longer than the other, and the bottom of the longer block was tapered for the purpose of collecting drops. The double-block system was attached to a frame in such a way that the vertical angle, and hence the flow rate through the channel, could be varied. The residence time/diffusion time of the viruses in the channel could thus be affected by the compression of the clamps as well as the channel angle.

The viruses considered for the calibration experiments were bacteriophages often employed in barrier-integrity tests (Lytle and Routson, 1995). The bacteriophages analyzed were ϕX174, PRD1, ϕ6, and MS2, with respective diameters of 27, 65, 80, and 24 nm. By comparison, the diameters of the human hepatitis B virus and human immunodeficiency virus are about 45 and 100 nm, respectively (Robinson, 1990; Wong-Staal, 1990). The virus concentration input into the channel reservoir was approximately 1.5×10^5 plaque forming units per ml. Physiologic saline, 0.16 Molar NaCl, was the carrier fluid for each of the viruses. In addition, calibration experiments were performed with PRD1 at various other salt concentrations ranging from 0.00016M to 1.6M.

Each calibration experiment was initiated by placing 2.0 ml of virus suspension in the reservoir at the top and allowing capillary action and gravity to fill the channel. The fluid exiting the channel formed drops at the tapered portion of the apparatus. Separate drops were timed and collected and their volumes measured, so that the channel flow rate was known as a function of time. Once a steady-state flow rate was achieved, three consecutive drops were saved and assayed in triplicate. The fluid in the reservoir was also sampled and assayed in triplicate. Details of the assay procedure are discussed elsewhere by Lytle *et al.* (1991). The average concentration of virus in the three drops taken from exit fluid was divided by the concentration in a sample of inlet fluid to form the relative transmission:

$$\text{Relative transmission} = \frac{\text{Average virus concentration in three drops at outlet}}{\text{Virus concentration at inlet}}. \tag{16}$$

Experiments were performed for a range of values of the relative time R, defined by:

$$R = \frac{\text{residence time of the virus within the apparatus}}{\text{time necessary for the virus to diffuse across the channel}}. \tag{17}$$

In terms of the channel parameters defined in the previous section [Table 1, equations (5c) and (6b)], the characteristic times for convection and diffusion are given by L/V_m and y_0^2/D_∞, respectively. Hence, for the calibration apparatus, R can be computed from

$$R = \frac{kTL}{2\pi y_0^4 a(-\partial p/\partial x)}. \tag{18}$$

The relative time is clearly a strong function of the channel height; variations in R over an entire order of magnitude were observed from natural variations in the clamping compression on the polycarbonate blocks. In the experiments the flow rate Q was measured and the channel half-height inferred indirectly from [see (5c)]

$$y_0 = \left(\frac{3\mu Q}{2w\rho g}\right)^{\frac{1}{3}}, \tag{19}$$

where ρ is the carrier-fluid density and w the channel width.

At each of the various experimental R values, a rate constant K was determined according to the procedure outlined at the end of Section 2. The average of all of these Ks constituted the rate constant reported for the particular virus interacting with latex in a saline medium of the prescribed salt concentration. The rate constants are given in Section 5.

4. VALIDATION EXPERIMENTS

The purpose of the validation experiments was to test the calibrated model under conditions as different as possible from those of the calibration procedure. We chose to compare the empirical and computational values of virus transmission through laser-drilled pores in condoms, using the virus PRD1 in physiological saline.

Holes were drilled in the tips of a batch of condoms using an excimer laser (Resonetics Inc., Nashua, NH). The exit holes were photographed and the hole diameters, ranging from about 1.7 to 2.7 μm, were recorded. The apparatus used

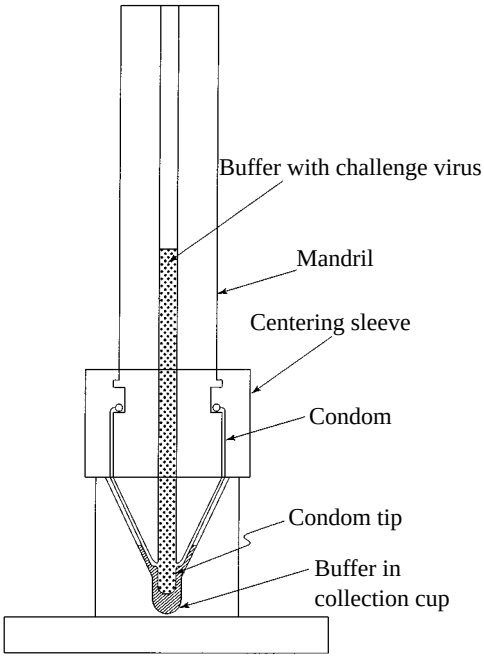

Figure 3. Apparatus used in validation experiments. Laser-drilled hole resides in tip of condom.

to measure the virus transmission is shown in Fig. 3. The condoms were filled with the virus suspension under a static pressure, and the viruses were transmitted to a collection fluid outside of the condom. The pressure difference imposed across the membrane corresponded to 5.5 cm of water (5394 dynes cm^{-2}). This relatively low pressure was required in order to keep the residence time in the pore at a high enough level (for the larger pores); otherwise the viruses simply sped through the pore with no opportunity to adsorb to the membrane.

In the experiments, the flux of virus into the pore was not easily measured, due to the miniscule volumes transmitted, so relative transmission of PRD1 was determined indirectly by simultaneously measuring the transmission of ϕX174. As ϕX174 displayed no adsorption in the calibration protocol, its concentration allowed for a convenient measure of 100% transmission. Dividing the collected concentration of PRD1 by the concentration of ϕX174 (both normalized by their initial concentrations since equal concentrations for each virus could not always be used) provided the value for relative transmission.

In previous studies with laser-drilled condoms (Lytle *et al.*, 1991; Mehta *et al.*, 1998), a high likelihood of cessation of the virus flow during experiments was discovered. This rather abrupt stoppage is apparently due to clogging by particulates released from the condom surface (Mehta *et al.*, 1998). Clearly, cessation of virus flow at an unknown time prior to the end of the collection period is a potential source of significant error. To circumvent this problem, separate collection fluids were assayed every 30 s. Data were used only when the amount of virus transmitted during

at least two consecutive periods was approximately the same and displayed no sign of reduced passage. This condition turned out to be quite difficult to achieve; evidence of at least partial clogging was seen in over 90% of the measurements. [Sometimes the flow ceased and later commenced again, consistent with the findings of Mehta *et al*. (1998).]

To simulate computationally the geometry of the laser-drilled pore, the diameter was assumed to be constant throughout the thickness of the membrane, at a value determined from the image of the exit hole. This is only an approximation, as the entrance holes where the laser strikes the membrane are known to be larger than the exit holes. It was also unknown to what extent the pore volume was free of debris. In order for the length of the pore to be accurately prescribed, the thickness of each membrane was measured at the pore location.

Computations in the circular-cylinder geometry required transformation of the governing equations into cylindrical coordinates. As the virus in the vicinity of the pore wall is modeled as a sphere near a plane, i.e., local curvature is ignored within the boundary layer, conversion to non-Cartesian geometries is straightforward. For example, equation (13) at the edge of the boundary layer applies in the cylindrical coordinate system (and other coordinate systems) once the normal derivative $\partial c/\partial y$ is replaced by the more general form $-\nabla c \cdot \boldsymbol{n}$ ($\boldsymbol{n}$ being the outward normal to the surface). Similarly, the resistance functions g_1 and g_2 for the velocity and diffusivity require no modification other than switching to the radial coordinate, since they are equal to one outside the boundary layer. The velocity profile of equation (5b) retains its parabolic shape for a circular cylinder, with centerline velocity equal to $(r_0^2/4\mu)(-\partial p/\partial x)$, (where r_0 is the cylinder radius). The computational method employed in the cylindrical coordinate system was identical to that described in Section 2 for the Cartesian system. The experimental and computational values of the amount of virus transported through the laser-drilled pores are given in the next section.

5. RESULTS

In this section we present the computational and experimental results used to develop, test and apply the model. Unless otherwise specified, the carrier fluid is saline at physiologic (0.16 Molar) salt concentration.

5.1. ***Selection of boundary-layer thickness.*** As noted in Section 2, solutions based upon the boundary-layer approach were compared to solutions to the full governing equations in order to determine the optimal boundary-layer thickness. It was found that for boundary-layer thicknesses between about one and three virus radii, the boundary-layer-based solution closely matched the full solution over the range of parameters tested. Figure 4 shows the virus concentration profile at the outlet of a parallel-sheet pore, derived from both the full equations and the reduced

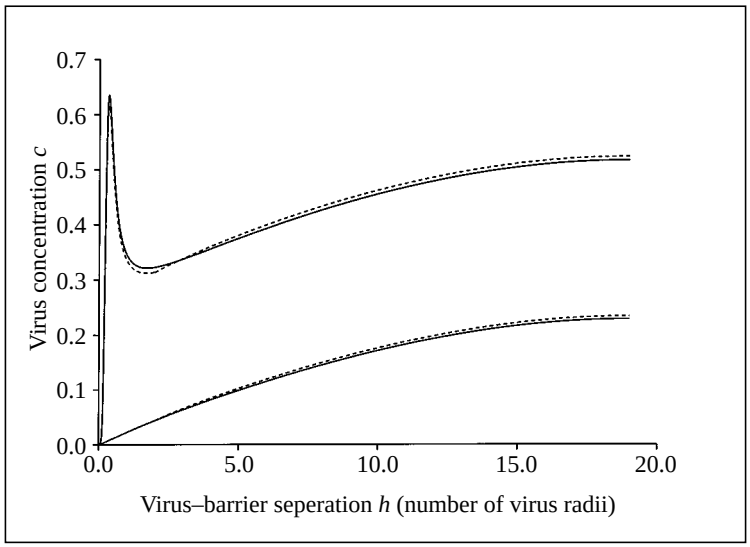

Figure 4. Virus concentration across the outlet face of a parallel-sheet pore. Solid lines represent solution to the full equations, assuming a Hamaker constant A of 2.2×10^{-20} J, and electrical potentials of $\Psi_1 = \Psi_2 = 24$ mV for the top curve, $\Psi_1 = \Psi_2 = 0$ for the bottom. The solution based upon the boundary-layer approach for each case is given by the dashed lines. Residence time/diffusion time = 1.0.

equations employing the boundary-layer thickness ultimately selected, 2.0 virus radii. All concentration values in Fig. 4 are normalized by the concentration c_0 at the pore inlet. The dashed lines represent the boundary-layer expression equation (10), for $h \leq 2$, and the solution to the outer equation (11) for $h \geq 2$. The separation between the sheets is 40 virus radii and the residence time/diffusion time for virus transport within the channel is 1.0. For the top two plots of Fig. 4, the Hamaker constant A is 2.2×10^{-20} J, and the electrical potentials assume the values $\psi_1 = \psi_2 = 24$ mV [representative values from other colloidal-particle applications (Ruckenstein and Prieve, 1976)]. For the lower two plots, the Hamaker constant is the same but the electrical potentials have been set to zero.

5.2. ***Rate constants.*** The data from the calibration experiments typically manifested the dependence upon R shown in Fig. 5. At small relative times the transmission decayed exponentially with R, while the falloff of relative transmission with R appears sub-exponential when R is greater than about 0.5. The corresponding K values were independent of R for $R < 0.5$ and decreased steadily with increasing R for $R > 0.5$. The reasons behind the observed dependence of K with relative time are discussed in the next section; here we simply note that the data in the range $R < 0.5$ were used to determine the K values.

The mean K values for the different viruses interacting with a latex membrane in physiologic saline are given in Table 2. The uncertainty estimates represent plus or minus one average deviation, where the average deviation is the sum of the

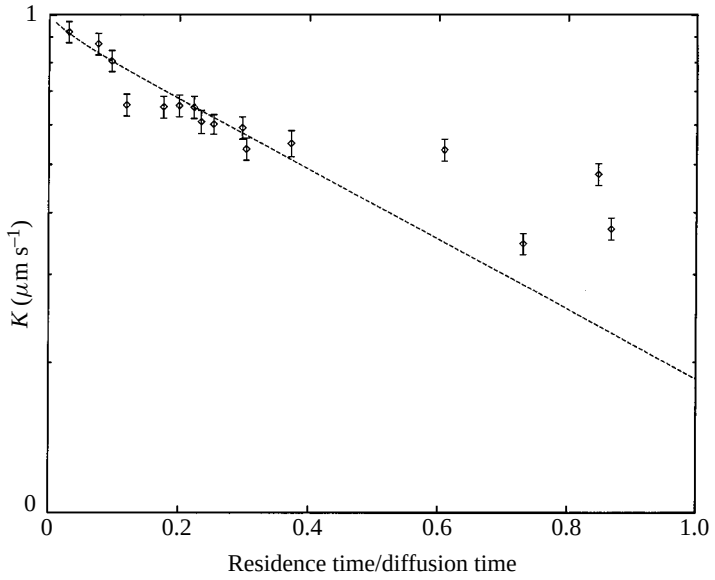

Figure 5. Relative transmission versus relative time for PRD1 transport in the calibration apparatus. Carrier fluid salt concentration is 0.16M.

differences (in absolute value) between each K value and the mean, divided by the number of K values. For ϕ6 and PRD1, there were some values of R for which the relative transmission was below that corresponding to the boundary condition $c = 0$, i.e., K was infinite. For the purpose of data analysis, at these data points the K value was clamped at the value given by the geometric mean of the three largest finite K values. While this procedure is somewhat arbitrary, it is important to note that beyond a certain K value, the relative transmission changes very little with variations in K, so the precise value of K is not critical. For example, considering PRD1 in 0.16M saline, the relative transmission is 0.61 for $K = 5\ \mu\text{m s}^{-1}$ and 0.59 for $K = 5000\ \mu\text{m s}^{-1}$. The uncertainties displayed in Table 2 are considerably larger than the individual-measurement errors (typically around 5%) signified by the error) bars in Fig. 5. While these uncertainties are rather large, we re-emphasize that a small difference in relative transmission is mapped into a large difference in associated rate constant, particularly when K is large.

The dashed curve in Fig. 5 is the prediction of the computer model for the relative transmission of PRD1 as a function of R, using $K = 2.85\ \mu\text{m s}^{-1}$ from Table 2 and $y_0 = 25\ \mu$m. Beyond a relative time of approximately 0.1, the dependence of the virus transmission upon relative time is seen to be exponential.

The role of the carrier-fluid properties on virus transport was studied by varying the salt concentration. The results plotted in Fig. 6 show three orders of magnitude variation in rate constant over the range of salinities examined, and a sharp change in the rate constant occurring around a concentration of 0.01M.

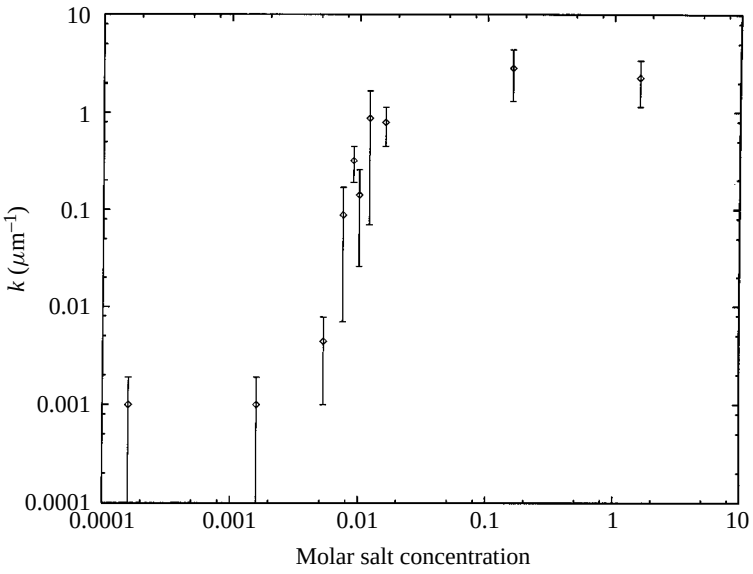

Figure 6. Rate constant versus salt concentration for PRD1 in saline interacting with a latex membrane.

Table 2. Rate constants for different viruses interacting with a latex membrane in 0.16M saline.

Virus	k (μm s^{-1})	Uncertainty in k (μm s^{-1})
ϕX174	0.02	0.02
MS2	0.25	0.19
PRD1	2.85	1.54
ϕ6	3.23	1.47

5.3. ***Model validation.*** A comparison of experimental and computational values of relative transmission of PRD1 through the laser-drilled holes is provided in Fig. 7. The length of the pores, i.e., the thickness of the condom, varied by almost a factor of two between the six trials represented in the figure. Thus it was useful to present the results as a function of relative time rather than pore diameter. The average difference between the measurements and model predictions is about 5%.

5.4. ***Example calculations.*** The implications of the wide variation in rate constants reported in Section 5.1 were assessed through some sample calculations based upon practical values for the input parameters. In one set of computations we imposed the standard (see Section 2) 80 000 dynes cm^{-2} pressure gradient across the membrane. The length of the pore was taken to be a typical thickness for a latex condom, 100 μm. Using 0.16M saline as the carrier fluid, we computed the relative transmission for our four bacterial viruses for cylindrical pores of various diameters. The smallest diameter considered was 0.4 μm, about five times the diameter

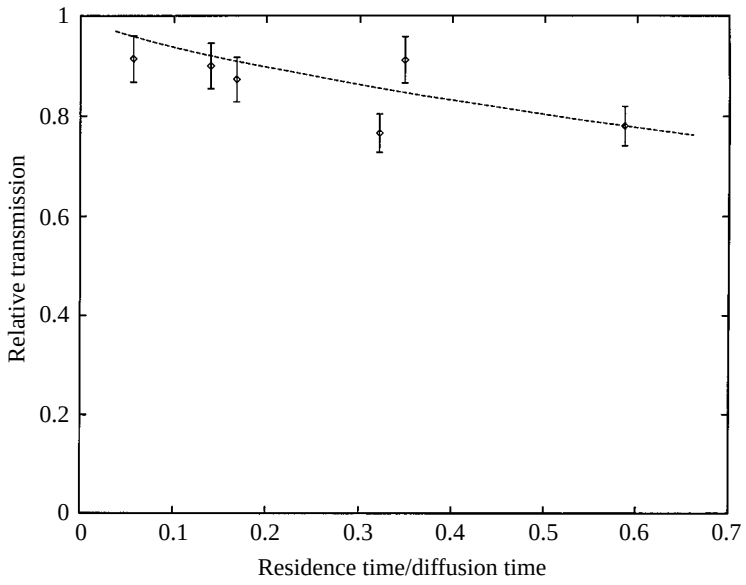

Figure 7. Relative transmission as a function of relative time for PRD1 passage through laser-drilled pores. Dashed curve represents predictions from computational model.

of largest virus, ϕ6, in order to satisfy the requirement that the pore diameter be much larger than the virus diameter. The transmission rates for the four viruses are plotted in Fig. 8. As the hole size is decreased, a sharp falloff in the transmission rate is seen for PRD1 and ϕ6, and a moderate falloff is observed for MS2, but there is virtually no decrease in the relative transmission for ϕX174 over the range of hole sizes considered.

Similar calculations (80 000 dynes cm^{-2} pressure, 100 μm pore length) performed for different values of the carrier-fluid ion concentration are summarized in Fig. 9. Here the virus is PRD1 and the pore diameter 0.5 μm. As the salinity of the carrier fluid is increased, a marked decrease in virus transmission is observed around a molar salt concentration of around 0.01, corresponding to the rapid change in rate constant at that salinity observable in Fig. 6.

6. DISCUSSION

The concentration profiles of Fig. 4 provide a view of the typical distribution of viruses across a pore. For the bottom curves, the interaction force between the virus and barrier is attractive at all virus–membrane separations. The virus velocity toward the wall induced by the interaction force increases as the separation decreases, and at a small enough separation the virus ceases to belong to the free-virus suspension. Appreciable adsorption occurs as the viruses traverse the pore; the

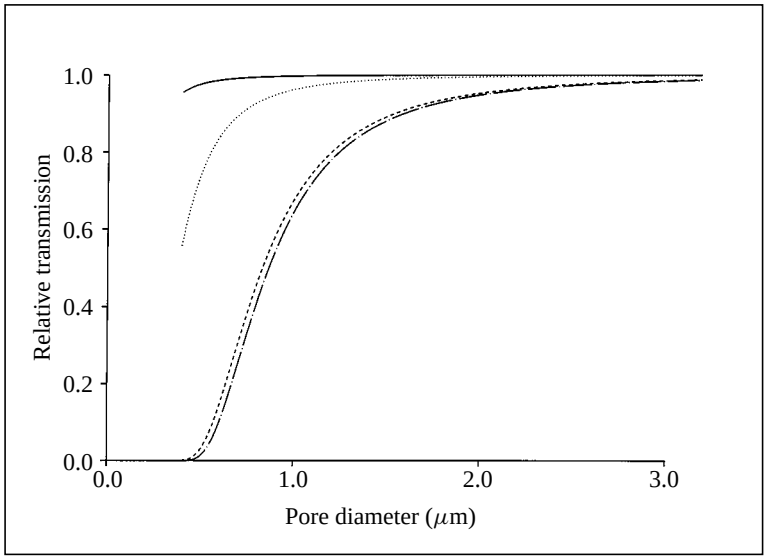

Figure 8. Relative transmission through cylindrical pores in a latex barrier versus cylinder diameter, for bacterial viruses ϕX174 (solid line), MS2 (dotted line), PRD1 (dashed line), and ϕ6 (dashed and dotted line). Pore length is 100 μm, driving pressure is 80 000 dynes cm^{-2}, and the carrier fluid is 0.16M saline.

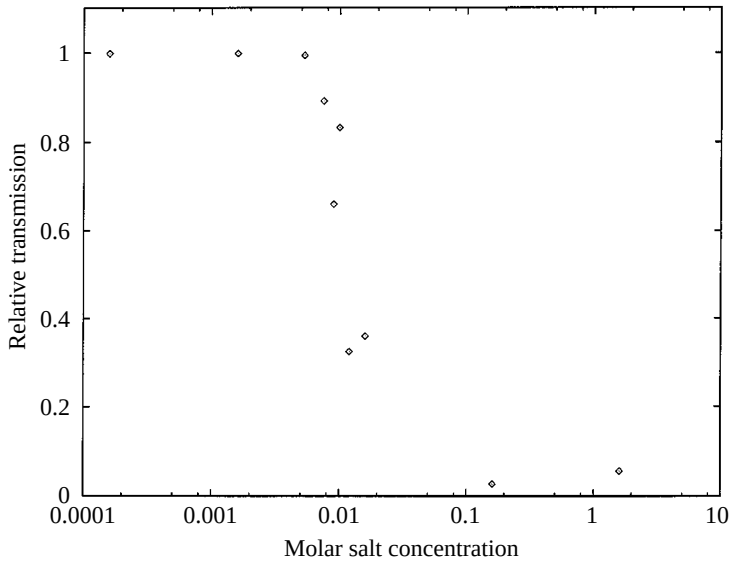

Figure 9. PRD1 transmission through a 0.5 μm diameter cylindrical pore, as a function of carrier-fluid salt concentration. Pore length is 100 μm and the driving pressure is 80 000 dynes cm^{-2}.

maximum concentration across the pore outlet is seen to be only about 0.2, compared with 1.0 at the inlet. For the top curves in Fig. 4, the virus–barrier interaction force is alternately attractive, repulsive, and again attractive as the separation distance

is increased. A potential energy barrier exists at around a separation of about 0.1 virus radii, along with an energy well just outside the barrier at a separation of around 0.3 radii. The virus concentration is highest in the potential-energy well. Owing to the presence of the repulsive electrical forces and hence the energy barrier, virus adsorption to the channel walls is appreciably less than for the purely attractive force.

The good agreement between the solid and dashed lines of Fig. 4 is evidence that the boundary-layer approach can provide accurate solutions to the transport equations. The advantage to the boundary-layer technique extends well beyond the computational efficiency relative to a full numerical solution. In the semi-empirical approach combined with the boundary-layer approximation, only a single empirical constant is determined, the rate-constant K. Solutions to the full transport equations incorporating the actual virus–membrane interaction forces require determination of three or more empirical constants. A multi-dimensional parameter-estimation problem is involved, solutions to which can be very laborious and subject to non-uniqueness issues. Perhaps most importantly, approaches incorporating the interaction forces are limited by the range of validity of the expressions describing the forces, and by the physical mechanisms included in the force expression. In the semi-empirical boundary-layer approach, all of the relevant physical mechanisms are contained within the parameter K.

For the experiments used to determine the K values, the eventual diminished rate of falloff in virus transmission with relative time, observable in Fig. 5 for $R > 0.5$, could reasonably be attributed to reversibility effects. That is, in addition to adsorbing to the pore wall, viruses are continually desorbing back into the suspension. For small values of transmission (high values of adsorption), the desorption flux would be significant. In experiments performed at a given R, i.e., a given separation distance y_0 in the calibration apparatus, reversibility would give rise to a time dependence of the relative transmission. (The steady state being an equilibrium between adsorption and desorption and a concomitant 100% transmission rate.) However, in additional experiments performed for durations more than twice that of the calibration experiments, the transmission rate remained steady (typically at a value of around 30% for PRD1) throughout the experiment. These extended-time experiments were performed with relative times in the range $1 < R < 3$, and hence were presumably affected by reversibility. Additionally, preliminary removal experiments indicate that essentially all of the untransmitted virus in a calibration experiment can be accounted for by rinsing the calibration apparatus after the experiment with the surfactant Tween 80, while none is recovered by rinsing with pure saline, indicating an essentially irreversible binding between the virus and latex in the presence of pure saline.

More than reversibility, dynamic adsorption (Van de Ven, 1989) appears to be a likely cause of the diminishing falloff in rate of transmission with large R. Van de Ven (1989) accounts both for viruses which are immobilized at the pore wall and those which are dynamically adsorbed, i.e., concentrated in a minimum of the

interaction energy between the virus and the pore wall, but still able to translate parallel to the wall. The dynamically adsorbed viruses contribute to the observed transmitted flux, especially when the axial flux through the central volume of the pore (outside the boundary layer) is relatively small. This immobilization reaction approximation of Van de Ven (1989), which requires the introduction of at least one additional empirical parameter, is currently being considered for its potential use in extending the perfect-sink-based model to smaller relative transmissions (higher adsorptions). For now, we restrict the quantitative application of the model to transmission rates above about 30%. Quantitative comparisons, say between different viruses or different carrier fluids, can be made at lower transmission rates. Examples of such comparisons are given below.

The exponential (linear on the semi-logarithmic scale) nature of the model prediction shown in Fig. 5 can be better appreciated by referring to previous solutions to related convective-diffusion problems. Under the conditions applicable to Fig. 5, the virus radius a is so much smaller than y_0 that the boundary condition (13) can be transferred to $y = 0$. After dividing through by Kc_0 in (13) the order of magnitude of the second term is $D_\infty/Ky_0 < 0.1$, so that (13) is well approximated by $c(x, 0) = 0$. If we further treat the diffusivity as constant in the outer region, the outer equations correspond to the classic Graetz problem (Eckert and Drake, 1972; Bowen *et al*., 1976). Following a developing region at small R, the concentration c and relative transmission decay exponentially with R. The solution for the concentration and relative transmission are actually an infinite series of exponentials, but for large Ky_0/D_∞ only the lowest-order mode is significant for relative times greater than about 0.05. For smaller values of K, e.g., for the virus MS2, a more complicated dependence upon R would be observed.

With regard to experimental validation of the model, the agreement between the model predictions and the measurements in Fig. 7 was felt to be good, especially given the amount of spread in the data points themselves. Part of the reason for the high accuracy of the model is the absence of the dynamic adsorption effect discussed above and evident for the calibration apparatus at a residence time of 0.5 (Fig. 5). That dynamic adsorption is still insignificant at a relative time of 0.7 demonstrates that the small-diameter cylindrical pore is much less efficient at adsorbing PRD1 virus than the parallel-sheet channel. For example, for a residence time/diffusion time of 0.5, the relative transmission is twice as high for the cylindrical pore. This might appear surprising, as a cylinder with the same radius as the channel half-width would be a more efficient adsorber than the channel. (For the parallel-sheet channel, Brownian motion in the direction out of the plane of Fig. 1 does not contribute to adsorption, making the channel less efficient at adsorption.) The higher transmission rate for the cylindrical pore than for the parallel-plate channel is due to the vastly different pore dimensions, in the following manner. Consider an axial location in each pore where a significant fraction of the pore cross-section has had a chance, via diffusion, to feel the effect of the boundary. This occurs where the relative time is $O(1)$ (e.g., 0.5), and is physically located much further in the axial

direction for the parallel-sheet channel than the cylinder. At this point an order of magnitude estimate for the concentration gradient $\partial c/\partial y$ is c_0/y_0 for the channel and c_0/r_0 for the cylinder (r_0 = cylinder radius). The dimensionless rate constants Ky_0/D_∞ and Kr_0/D_∞ then provide a measure of the adsorptive tendencies of the systems. We see that in a normalized sense the cylinder has a smaller rate constant and is less adsorptive, even though for $Ky_0/D_\infty = Kr_0/D_\infty$ the cylinder would be more adsorptive.

The very different rate constants in Table 2 are indicative of the very different adsorption tendencies for the four viruses studied. PRD1 and ϕ6 are highly adsorptive to latex at physiologic salt concentrations, MS2 is moderately adsorptive, and to within experimental accuracy no adsorption of ϕX174 to latex was ever observed. An important practical implication of the wide range of adsorptive behavior exhibited by the test viruses can be seen from Fig. 8. As expected for large hole sizes, the residence time was too small for appreciable adsorption to occur, and each virus had an asymptotic relative transmission value of 1.0. However, for small-diameter pores the transmission rate was highly virus-dependent. While the very low transmission rates should be recognized as underpredictions (as discussed at the beginning of this section), it is clear that assessing barrier integrity based upon transmission rates for PRD1 or ϕ6 would lead to a gross underestimation of the probability of transmission for a virus similar to ϕX174.

Potentially misleading test results can also occur under circumstances where the ion concentration of the laboratory carrier fluid is different from that occurring in practice. The results of Fig. 6 show a significant influence of salt concentration on the rate constant for PRD1 with a latex membrane. The small rate constants at low salt concentrations demonstrate that the repulsive electrical forces, which are unshielded (Hiemenz, 1986; Israelachvili, 1992) due to the low ion concentration, allow little adsorption, i.e., boundary condition (13) reduces to the virus-conserving condition $D(y)\partial c/\partial y = 0$ at $y = y_{bl}$. The opposite is true at high salt concentrations: the free ions effectively neutralize the electrical forces and, under the influence of the dominant van der Waals force, an essentially perfect sink–boundary condition $c = 0$—is present even at the edge of the boundary layer. The practical importance of the ion-concentration level is manifested in Fig. 9: a probability of virus transmission based upon results obtained with 0.16M saline would not be representative of the risk associated with use of the membrane in a low-salt environment. A striking feature of Fig. 9 is how sharply the division between high transmission and low transmission occurs. Within a factor of two on either side of 0.01M, the transmission varies by an order of magnitude. (Again, the lowest transmission values are probably underestimated within the perfect-sink approximation.) The transmission values plotted in Fig. 9 apply to a single pore diameter, driving pressure, pore length, etc. The transmission values at higher salt concentrations would be higher, for example, for larger-diameter pores. One important role of the computational model is to provide a quick estimate of the risk of virus transmission for any parameter combination of interest.

7. CONCLUSIONS

In this paper a boundary-layer approximation to the particle-transport equations has been used to develop a model for simulating virus transport through barriers. The model is quantitatively applicable for $O(1)$ values of the relative transmission. For very small values of relative transmission the amount of virus adsorption is over-predicted, probably due to the small but finite velocity of the dynamically adsorbed viruses which are ignored within the perfect-sink approximation but contribute to the flux through the pore. Even for low values of the virus transmission, the model is useful for qualitative comparisons of the likelihood of transmission between different viruses and different carrier fluids.

An important consequence of the boundary-layer approach is the emergence of a single rate constant characterizing the complex physical interaction between the virus and the barrier in the presence of a carrier fluid. The rate constants are universal - they apply to the vast majority of pore flows, where Brownian motion and interaction forces are the dominant transport mechanisms near the pore walls. (A counterexample would be a situation where carrier fluid is sucked through the pore boundary at a sufficiently high rate.) Successful application of the model requires knowledge of the rate constant K for each virus–barrier–carrier-fluid combination of interest. The most novel feature of the model is the empirical determination of K in an apparatus which allows for measurable amounts of virus adsorption as well as rapid simulation of transport through the device.

While the mathematical model was derived and applied in simple geometries, it can be readily extended to more complicated configurations. Elliptical cylinders provide reasonable geometric approximations to slits or tears that occur in surgical and examination gloves. Tortuous-path geometries, or arrays of bodies (e.g., spheres), are more appropriate for modeling natural material porosity. Within the array model, allowance must be made for the hydrodynamic interaction between the virus and the boundary in a local stagnation-point flow, rather than the purely shear flows considered in this paper.

At this time the model is restricted to steady-state simulations. Incorporation of a time-varying pressure gradient, as would be present in realistic simulations of sexual or surgical behavior, is conceptually straightforward once an estimate of the transient pressure can be made. A much more difficult transient effect to incorporate is capillary action. (The presence of the free surface complicates the simulation.) In some cases surface tension dictates whether the steady-state flows assumed to exist are actually initiated, as the driving pressure must exceed the tension of the fluid surface extending across a pore opening. Surface tension also strongly affects the time necessary for the concentration front to negotiate the pore. Analysis of capillary action will require further empirical information, particularly about the interaction energy between the carrier fluid and the barrier material. Inclusion of both transient pressures and surface-tension effects is a long-term goal of the modeling effort.

The practical value of the simulation model will be enhanced as calibration is performed for other virus–barrier–carrier fluid combinations of interest; i.e., as the database of rate constants is enlarged. Efforts are underway to include two viruses of high public-health interest, herpes and HIV. An additional goal is to perform calibration experiments using serum, the major constituent of blood and semen, as the carrier fluid. New barrier materials, not only for elastic membranes but for gowns, masks, and biomedical filters, are rapidly being developed. It is our hope that the mathematical model can be calibrated on an ongoing basis to include these materials, so that assessment of the integrity of the materials as barriers to virus transmission can be performed under a wide range of use conditions.

ACKNOWLEDGEMENTS

The authors with to thank the Office of Women's Health of the U. S. Food and Drug Administration for financial support of this project. We are also grateful to the Division of Electronics and Computer Science of FDA/CDRH for computer support, in particular the assistance of Dr Jonathon Boswell. Finally, we wish to acknowledge the reviewer's comments regarding the potential importance of reversibility effects in explaining the trends within the calibration data.

REFERENCES

Adamczyk, Z. and T. G. M. Van De Ven (1981). Deposition of particles under external forces in laminar flow through parallel-plate and cylindrical channels. *J. Colloid Interface Sci.* **80**, 340–356.

Bowen, B. D., S. Levine and N. Epstein (1976). Fine particle deposition in laminar flow through parallel-plate and cylindrical channels. *J. Colloid Interface Sci.* **54**, 375–390.

Brenner, H. and L. G. Leal (1977). A model of surface diffusion on solids. *J. Colloid Interface Sci.* **62**, 238–258.

Brenner, H. and L. J. Gaydos (1977). The constrained Brownian movement of spherical particles in cylindrical pores of comparable radius. *J. Colloid Interface Sci.* **58**, 312–356.

Carey, R. F., W. A. Herman, S. M. Retta, J. E. Rinaldi, B. A. Herman and T. W. Athey (1992). Effectiveness of latex condoms as a barrier to human immunodeficiency virus-sized particles under conditions of simulated use. *Sex. Transm. Dis.* **19**, 230–234.

Chari, K. and R. Rajagopalan (1985). Deposition of colloidal particles in stagnation-point flow. *J. Chem. Soc. Faraday Trans. 2.* **81**, 1345–1366.

Eckert, E. R. G. and R. M. Drake (1972). *Analysis of Heat and Mass Transfer*. New York: McGraw-Hill.

Goldman, A. J., R. G. Cox and H. Brenner (1967). Slow viscous motion of a sphere parallel to a plane wall - II Couette flow. *Chem. Eng. Sci.* **22**, 653–660.

Hiemenz, P. C. (1986). *Principles of Colloid and Surface Chemistry*, 2nd edition. New York: Marcel Dekker.

Hogg, R., T. W. Healy and D. W. Fuerstenau (1966). Mutual coagulation of colloidal dispersions. *Trans. Faraday Soc.* **62**, 1638.
Israelachvili, J. N. (1992). *Intermolecular and Surface Forces*, 2nd edition. San Diego, CA: Academic Press.
Jia, X. and R. A. Williams (1990). Particle deposition at a charged solid/liquid interface. *Chem. Eng. Comm.* **91**, 127–198.
Lytle, C. D., A. P. Budacz, E. Keville, S. A. Miller and K. N. Prodouz (1991). Differential inactivation of surrogate viruses with merocyanine 540. *Photochem. Photobiol.* **54**, 489–493.
Lytle, C. D. and L. B. Routson (1995). Minimized virus binding for tests of barrier materials. *Appl. Environ. Microbiol.* **61**, :643–649.
Lytle C. D., L. B. Routson, J. E. Duff, B. Fleharty and W. H. Cyr (1997). A sensitive method to evaluate condoms as virus barriers. *J. AOAC Int.* **80**, 319–324.
Mehta, R. I., C. D. Lytle, D. P. Thomas and M. R. Myers (1998). The cause of cessation of viral passage through holes in latex condoms. *J. Rubb. Res.* **1**, 1–13.
Numerical Algorithms Group Limited (1991). *The NAG Fortran Library Manual, Mark 15*, Oxford: NAG.
Probstein, R. F. (1994). Physicochemical Hydrodynamics An Introduction. 2nd edition. New York: John Wiley.
Prieve, D. C. and M. M. J. Lin (1980). Adsorption of Brownian hydrosols onto a rotating disk aided by a uniform applied force. *J. Colloid Interface Sci.* **76**, 32–47.
Rajagopalan, R. and J. S. Kim (1981). Adsorption of Brownian particles in the presence of potential barriers: effect of different modes of double-layer interaction. *J. Colloid Interface Sci.* **83**, 428–448.
Robinson, W. S. (1990). Hepadnaviridae and their replication, in *Virology*, 2nd edition, B. N. Fields, D. M. Knipe *et al*. (Eds), New York: Raven Press, Chap. 76.
Ruckenstein, E. and D. C. Prieve (1976). Adsorption and desorption of particles and their chromatographic separation. *AIChE J.* **22**, 276–283.
Song, L. and M. Elimelech (1995). Particle deposition onto a permeable surface in laminar flow. *J. Colloid Interface Sci.* **173**, 165–180.
Van De Ven, T. G.'M. (1989). *Colloidal Hydrodynamics*. San Diego, CA: Academic Press.
Wong-Staal, F. (1990). Human immunodeficiency viruses and their replication. in *Virology*, 2nd edition, B. N. Fields, *et al*. (Eds), New York: Raven Press, Chap. 53.

Received 21 December 1997 and accepted 22 October 1998